Structural Engineering and Mechanics, *Vol. 73, No. 6 (2020) 651-666*
DOI: https://doi.org/10.12989/sem.2020.73.6.651

Practical coherency model suitable for near- and far-field earthquakes based on the effect of source-to-site distance on spatial variations in ground motions

Rui-Fang Yu[1], Abduwahit Abduwaris[2] and Yan-Xiang Yu*[1]

[1]*Institute of Geophysics, China Earthquake Administration, Beijing, China*
[2]*Earthquake Administration of Xinjiang Uyghur Autonomous Region, Wulumuqi, China*

(*Received April 2, 2019, Revised October 29, 2019, Accepted November 12, 2019*)

Abstract. In this study, the spatial variation mechanisms of large far-field earthquakes at engineering scales are first investigated with data from the 2008 Ms 8.0 Wenchuan earthquake. And a novel 'coherency cut-off frequency' is proposed to distinguish the spatial variations in ground motions in the low-frequency and high-frequency ranges. Then, a practical piecewise coherency model is developed to estimate and characterize the spatial variation in earthquake ground motions, including the effects of source-to-site distances, site conditions and neighboring topography on these variations. Four particular earthquake records from dense seismograph arrays are used to investigate values of the coherency cut-off frequency for different source-to-site distances. On the basis of this analysis, the model is established to simulate the spatial variations, whose parameters are suitable for both near- and far-field earthquake conditions. Simulations are conducted to validate the proposed model and method. The results show that compared to the existing models, the proposed model provides an effective method for simulating the spatial correlations of ground motions at local sites with known source-to-site distances.

Keywords: spatial variation; coherency function; dense seismograph array; UPSAR; Wenchuan earthquake; Parkfield earthquake; San Simon earthquake

1. Introduction

Ground motion is known to display complex variation patterns in space and time. Earthquake engineers have focused their attention on the temporal variations in ground motion, such as the time history characteristics of acceleration, which are fundamental factors in dynamic analysis and the seismic design of buildings. However, many studies have revealed that the spatial variations of seismic ground motions are the main sources of the seismic forces that act on underground structures such as bridge supports, subways, pipelines, tanks, and similar structures that extend for large distances and are widely spaced (Hindy and Novak 1980, Sayed *et al*. 2015, Tian *et al.* 2018, Yurdakul and Ates 2018). Individual supports of extensive structures undergo different motions during an earthquake, which can increase the response of a structure beyond the expected response if the earthquake inputs at the structural supports are assumed identical (Saxena *et al.* 2000, Zerva 2009, Bilici *et al*. 2009, Mohamed *et al*. 2015, Tonyali *et al.* 2019). The spatial variations in ground motion can be described by the normalized cross-power spectrum, which can illustrate the relationships among different stochastic processes in the frequency domain and is easily applied. Novak *et al*. (1980) first proposed a coherency model in earthquake engineering based on the coherency model of wind and utilized the model in pipeline research. Fen and Hu (1981) constructed a coherency model by analyzing recordings from the 1975 Haicheng earthquake. Later, more trustworthy coherency function models were presented by researchers around the world based on the abundant and valuable recordings from the Strong Motion Array Taiwan (SMART-1) (Bolt *et al*. 1982, Lou 1985, Harichandran and Vanmarcke 1986, Abrahamson *et al*. 1991, O1iveira *et al*. 1991, Qu *et al*. 1996). In addition, some semitheoretical and semiempirical models of the spatial coherency functions of ground motion have been proposed based on research on the frequency spectrum of ground motion (Luco and Wong 1986, Der Kiureghian 1996, Zerva and Harada 1997, Ding *et al.* 2004, Yu *et al*. 2011). These models have been widely used to simulate spatially varying ground motions and to calculate the dynamic responses of large-span structures under different earthquake inputs for individual supports (Luco and Wong 1986, Hao *et al*. 1989, Jankowski and Wilde 2000, Amiri and Bagheri 2009, Konakli *et al*. 2012, Hu and Xu 2012, Wu *et al*. 2016, Liu *et al*. 2017). In fact, these theoretical and empirical coherency models assume that the site characteristics are fully deterministic and homogeneous, but this assumption is not compatible with the observations from array data (Somerville *et al*. 1991). With the increase in dense seismograph array data, some factors that affect ground motion spatial variations can now be determined, such as the source mechanism, propagation path and site conditions (Somerville *et al*. 1999, Liao *et al*. 2007). The effects of irregular topography and local site conditions on the coherency functions of spatial ground motions obviously cannot be neglected (Zerva and Harada 1997, Liao and Li 2002, Bi and Hao 2011). Nevertheless, at

*Corresponding author, Professor
E-mail: yuyx@cea-igp.ac.cn

http://www.techno-press.com/journals/sem&subpage=7
ISSN: 1225-4568 (Print), 1598-6217 (Online)

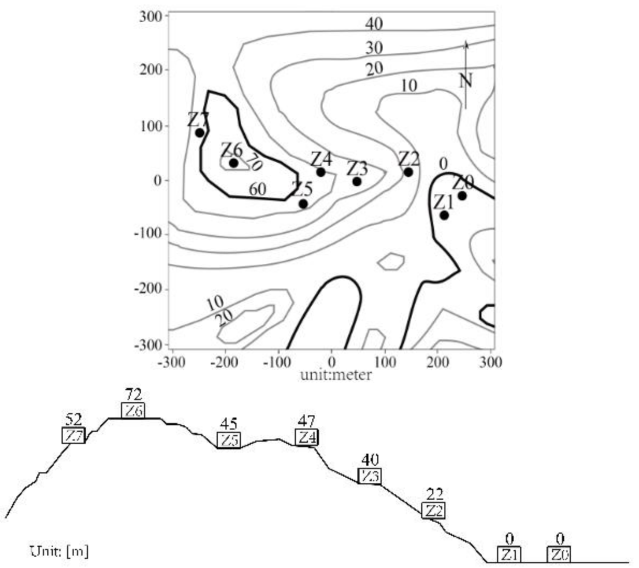

Fig. 1 The stations distribution of the Zigong Seismograph Array

present, recorded spatial ground motion data from sites with different conditions are limited. These coherency models are not fully adequate for simulations spatial variation in ground motion considering different conditions, including the neighboring topography, local site conditions, and source-to-site distance (Bi and Hao 2012). Although some simulated data can also be used to study the spatial variation in ground motions (Chaouch *et al*. 2016, Gade and Raghukanth 2018), many human factors are included in the simulated results. Therefore, new and detailed recorded data are needed, especially from large earthquakes, to accurately analyze the spatial variations in earthquake motion. Fortunately, the Zigong Seismograph Array (ZGSA) recorded strong ground motions during the 2008 Wenchuan earthquake (Ms 8.0).

The ZGSA is a dense seismograph array that was installed in Sichuan Province, China, in 2007 to observe the effect of topography. The ZGSA includes eight irregularly spaced seismograph stations, as shown in Fig. 1. Each station is equipped with a three-component force-balance accelerometer (FBA), and each channel is digitized at 18 bits and 200 samples per second. These stations are spaced irregularly, with interstation spacing ranging from 47 m to approximately 385 m. There is a 72 m elevation difference between the lowest station (Z0 or Z1) and the highest station (Z6). Station Z0 is located on a soil site, and the remaining stations are located on rock sites. The data can be used to analyze the influence of different site conditions and neighboring topography on the coherency loss of spatial ground motions. Moreover, ZGSA is of the same scale order as large engineering structures, and the distance to the epicenter of the Wenchuan event is approximately 226.6 km. Therefore, these data are of great value in studying the spatial variations in ground motion at the engineering scale, especially the spatial variations of a large far-field earthquake.

The main objective of this study is to show the station-to-station variations in ground motion during the Wenchuan event, as recorded by ZGSA. First, we show the variations in some parameters based on the relevant records. These parameters include the amplitude spectra, coefficients of variation, peak values and vertical-to-horizontal response spectra ratios. Second, we analyze the variation mechanisms of the lagged coherency functions of these records with the station-to-station distance and frequency changes. Third, we discuss the factors that influence the spatial variations of ground motion, such as different site conditions and neighboring topography effects. Fourth, we define the 'coherency cut-off frequency' to explain the

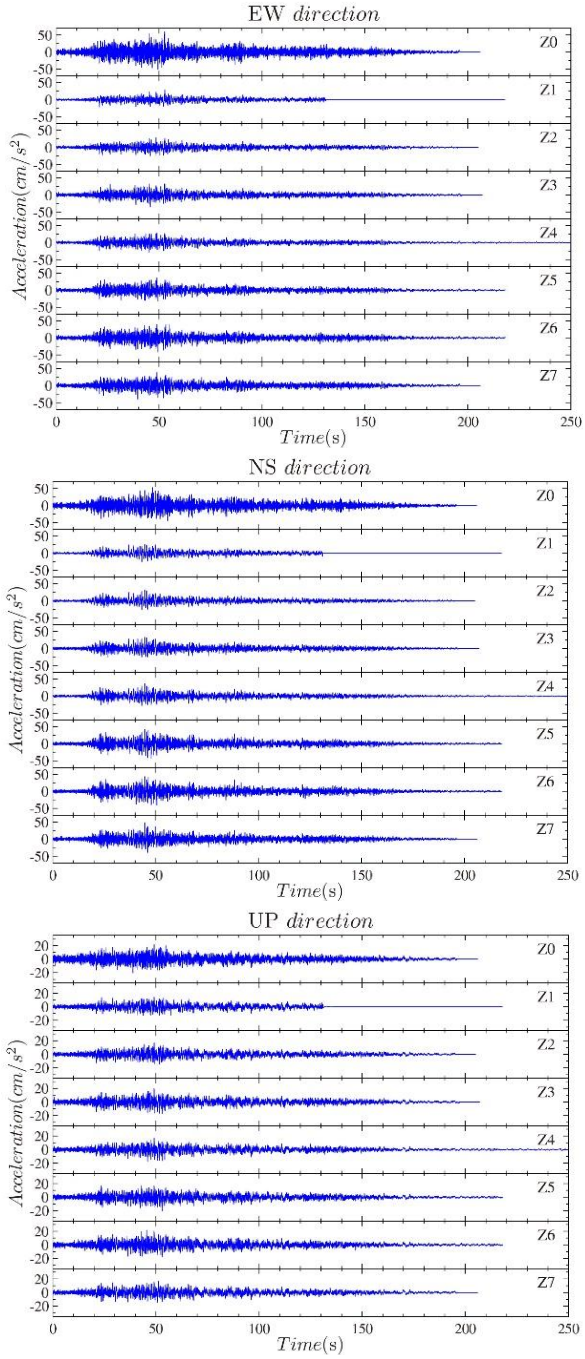

Fig. 2 Acceleration time series of east-west (EW), north-south (NS) and up-down (UP) components recorded by ZGSA during 2008 Wenchuan earthquake

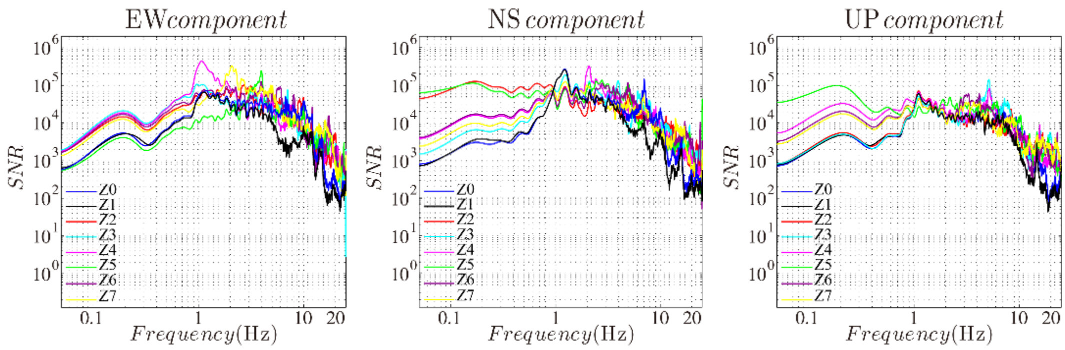

Fig. 3 Signal-to-noise ratios for three components of the 8 stations of ZGSA

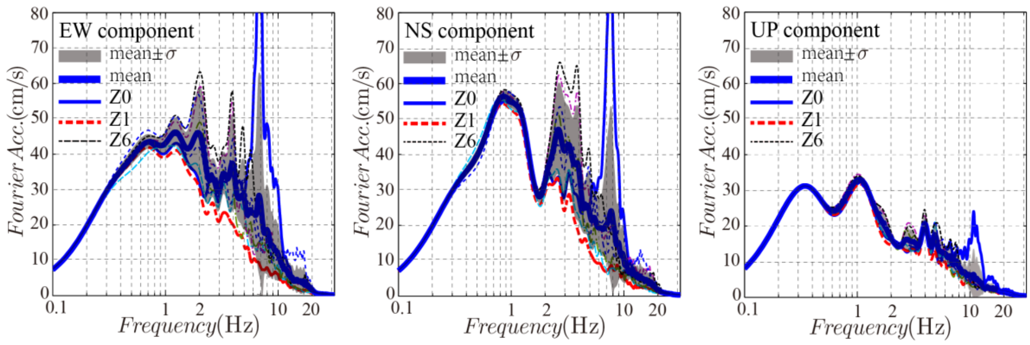

Fig. 4 Plots illustrating smoothed three-component Fourier amplitude spectra observed at the ZGSA stations during the Wenchuan earthquake. The heavy lines represent the spectral mean of the recordings of the eight stations, and the gray bands represent the variance range from *mean-σ* to *mean+σ*, where *σ* is the standard deviation

effect of the source-to-site distance on spatial variations in ground motion. Finally, we establish a piecewise model based on the coherency cut-off frequency to simulate the variation in the lagged coherency of ground motions, which is suitable for the conditions of a strong earthquake in the near and far fields. This model can be used in simulations of spatially correlated multipoint ground motions at sites with known distances to the epicenter. Although well supported by data, many of our observations are qualitative because of the complexity of ground motions.

2. Observed ground motion variations

The acceleration time series from the Wenchuan earthquake recorded by the ZGSA are plotted in Fig. 2, including the east-west (EW), north-south (NS) and up-down (UP) components. The signal-to-noise ratios (SNRs) of recordings, defined as the ratio of the Fourier amplitude of signal to noise, are calculated primarily to test the reliability of signals, in which random noise is the time series before the first *P*-wave arrival of the recording. The SNRs of recordings for three components are shown in Fig. 3. Notably, these signals are reliable at frequencies ranging from 0.05 Hz to 35 Hz. Moreover, because most digital recordings are plagued by random baseline offsets, baseline correction must be performed on acceleration records before these data are used to study the spatial variations in ground motion. Some studies of earthquakes in Taiwan and California have implied that ground motions with periods of less than approximately 20 s are usually unaffected by specific baseline correction schemes (Boore 2001, Wang *et al*. 2003, 2006). Thus, we applied a simple baseline correction scheme in this study. First, the mean of the entire record was removed from the whole record. Then, an acausal fourth-order Butterworth high-cut filter with a cut-off frequency of 0.05 Hz was applied to each record.

2.1 Fourier amplitude spectra

The Fourier amplitude spectra of acceleration recorded by the eight stations of ZGSA during the 2008 Wenchuan event are illustrated in Fig. 4, which includes the variation curves of the EW, NS and UP components. The spectra were smoothed using a 5-point smoothing function repeated three times. Assuming the frequency interval is 0.5 Hz, then 70 discrete frequencies can be obtained between 0.1-35 Hz. For each given frequency, the mean and standard deviation *σ* of Fourier amplitudes can be obtained by analyzing 8 results in each direction. The heavy lines in Fig. 4 represent the spectral means of the recordings of the eight stations, and the gray bands represent the variance range from *mean-σ* to *mean+σ*. The following trends can be seen in the figure.

(1) The dominant frequency observed is different for each station. The Fourier amplitudes of recordings from station Z0, plotted with solid lines, are obviously larger than those of other stations, ranging from 7-11 Hz. This difference is likely caused by different site conditions, particularly at Z0. The effect of site conditions on the horizontal components is larger than that on the vertical component.

(2) If the effect of recordings from station Z0 is ignored,

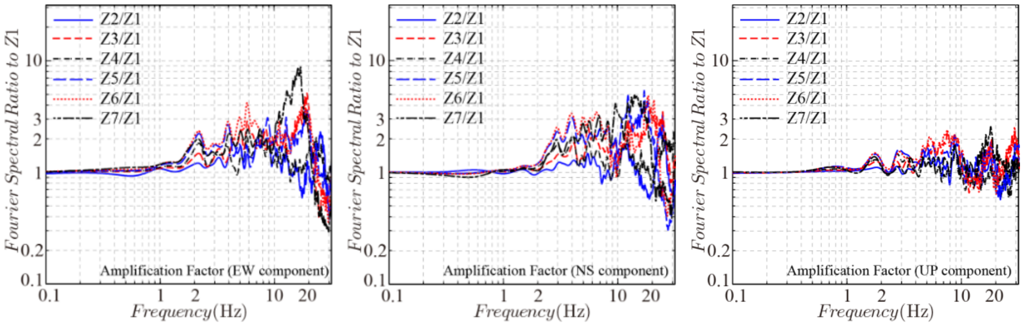

Fig. 5 Fourier spectral ratios between stations Z2-Z6 and station Z1 for three components

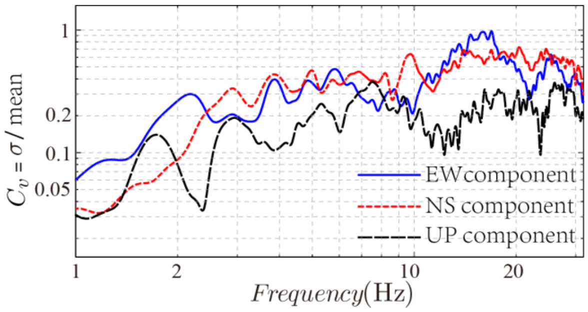

Fig. 6 Coefficient of variation for the Fourier spectra observed from the Wenchuan earthquake

the Fourier amplitude of recordings from station Z1 is lower than the gray band, and the value of recordings from station Z6 is higher than the gray band. We suspect that this variation may relate to interstation elevation differences. If we regard station Z1 as a reference point, then the ratio of the Fourier amplitude spectra of recordings at stations Z2-Z6 and Z1, i.e., the amplification factor, can be used to analyze the effect of interstation elevation differences, as shown in Fig. 5, in which the data from station Z0 are excluded. Clearly, the variation depends on the frequency f. When $f \leq 1.0$ Hz, the amplification factor is close to 1.0, and when 1.0 Hz$\leq f \leq$8.0 Hz, the amplification factor increases gradually with increasing elevation difference. However, in the high-frequency range, no obvious relationships appear between the amplification factor and elevation difference. These results show that the acceleration amplitude may be amplified with increasing interstation elevation differences, but in the high-frequency range, more complex effects exist. Furthermore, the amplifying action of increasing elevation difference has a larger effect in the horizontal directions than in the vertical direction.

To better understand the variation in ground motion as a function of frequency, we computed the coefficient of variation (C_v) of the Fourier spectra, which provides a relative measure of data dispersion compared to the mean

$$C_v = \sigma / mean \times 100\% \tag{1}$$

When C_v is small, the data scattering relative to the mean is small, and when C_v is large, the data scattering relative to the mean is large. Since station Z0 is located on the soil site, the data from station Z0 are excluded in the calculation of C_v, that is, the corresponding mean and σ for each frequency are the results of stations Z1-Z7. Fig. 6 illustrates the C_v values of three components as a function of frequency.

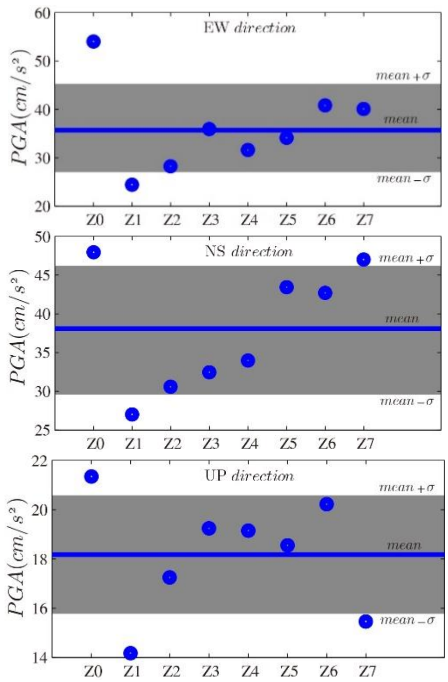

Fig. 7 The variations in PGA for the recordings observed from the Wenchuan earthquake. The heavy lines represent the mean PGAs of the recordings at the eight stations, and the gray bands represent the variance ranges from *mean*-σ to *mean*+σ, where σ is the standard deviation

Notably, C_v generally increases with increasing frequency. The source-to-site distance of the Wenchuan event is approximately 226.6 km, and we suspect that many of the high frequencies may have been depleted before arriving at ZGSA. As a result, the C_v of the Wenchuan event is relatively small. In contrast, the coefficients at frequencies larger than 3.0 Hz are large. Additionally, the variations of ground motions depend on the direction of the ground motion. The C_v values of vertical components are systematically smaller than those of the two horizontal components, except in the frequency range of 7-9 Hz. However, for the two horizontal components, the coefficients are only slightly different.

2.2 Peak values of recordings

The peak ground accelerations (PGAs) recorded at stations Z0-Z7 are plotted in Fig. 7, in which the heavy lines indicate the PGA mean of the recordings at the eight

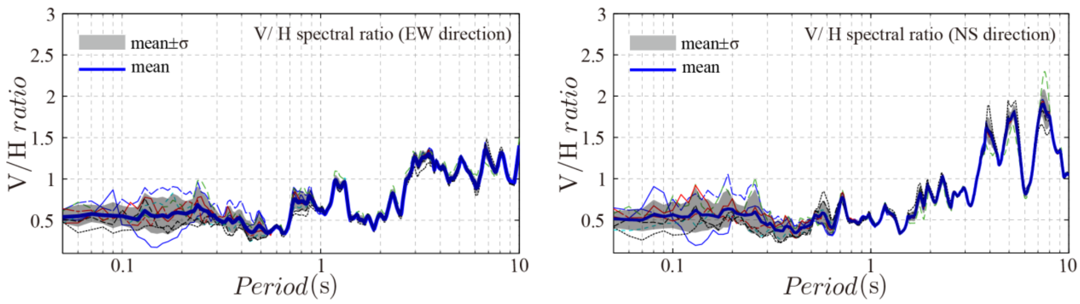

Fig. 8 Plots showing the response spectral ratio of vertical to horizontal components as a function of period. The bold line indicates the mean of V/H ratios from eight records, and the gray band indicates the variance range from *mean-σ* to *mean+σ*, where *σ* is the standard deviation

stations and the gray bands represent the variance range from *mean-σ* to *mean+σ*, where *σ* is the standard deviation. Clearly, very significant station-to-station variations occur among the PGAs from each record, although the maximum distances between stations are less than 400 m. For instance, the separation distance between Z0 and Z1 is approximately 52 m, but the values of PGAs are obviously different, which shows that the local site conditions affect the acceleration amplitudes. Furthermore, the variations in PGAs with increasing station elevation are obvious in the horizontal directions but not in the vertical direction because of the complexity of high-frequency in ground motion, as shown in Fig. 7.

2.3 Vertical-to-horizontal response spectral ratio

The vertical-to-horizontal (*V/H*) response spectral ratio is defined as the ratio of the 0.05 damping response spectrum in the vertical and horizontal directions in a series of discrete periods. The ratio is found to depend strongly on the period and source-to-site distance (Bozorgnia and Campbell 2004, Wang *et al*. 2006, Bradley and Cubrinovski 2011). Fig. 8 shows the variation in the *V/H* response spectral ratio based on the period, in which, the bold line indicates the mean *V/H* ratio from the eight records, and the gray band indicates the variance range from *mean-σ* to *mean+σ* (*σ* is the standard deviation). Generally, the *V/H* response spectral ratio is high in the near-field region and in the high-frequency range, and the most common V/H response spectral ratio is equal to approximately 2/3. In contrast, for far-field earthquakes, the mean value of *V/H* spectral ratios is approximately 0.5 when the period ranges from 0.05-1.0 s. Beyond this range, the ratios increase gradually with increasing period. Moreover, the *V/H* response spectral ratio of station Z0 (located on a soil site) is obviously smaller than those of other stations from 0.1 - 0.2 s, and the data scattering relative to the mean is larger in high-frequency ranges. Therefore, local site conditions have considerable effects on the *V/H* response spectral ratio, and the source-to-site distance affects variations in the ratio based on the period.

3. Lagged coherency of ground motions

For a stationary process, the cross-covariance function of the motions between two stations is defined as in Eq. (2) (Jenkins and Watts 1969)

$$\hat{R}_{mn}(t) = \frac{1}{T}\int_0^{T-|\tau|} y_m(t) y_n(t+\tau)\,dt \qquad |\tau| \le T \tag{2}$$

where $y_m(t)$ and $y_n(t)$ are two time-series of recordings in the same direction, τ is the time lag. Let the duration of the strong-motion S-wave window be $0 \le t \le T$, where $T = N\Delta t$, N is the number of samples in the recorded time series for the window, and Δt is the time step. Notably, the window of the actual time history is assumed to be a segment of an infinite window with uniform characteristics through time (stationarity assumption). The cross-covariance function is generally smoothed before it is further used as an estimator, and this function is given as follows

$$R_{mn}(\tau) = \mathrm{w}(\tau)\hat{R}_{mn}(\tau) \tag{3}$$

where $\mathrm{w}(\tau)$ is the lag window with properties $\mathrm{w}(\tau)=\mathrm{w}(-\tau)$, $\mathrm{w}(\tau=0)=1$ and $\int_{-\infty}^{\infty}\mathrm{w}(\tau)=1$.

Then, the smoothed spectral density (or cross spectrum) of the process is evaluated as follows

$$S_{mn}(\omega) = \frac{1}{2\pi}\int_{-T}^{T} R_{mn}(\tau)\,\mathrm{e}^{-i\omega\tau}\,d\tau \tag{4}$$

where $i=\sqrt{-1}$ and ω is the angular frequency (in rad/sec).

The Fourier spectra of the ground motions at various stations are obviously not identical. However, the assumption of spatial homogeneity in the random field implies that the power spectrum of motion is independent of station (Zerva 2002). Then, the coherency of ground motion is obtained from the smoothed cross spectrum of motion between two stations m and n, and the spectrum is normalized based on the corresponding power spectra (Hindy and Novak 1980, Harichandran and Vanmarcke 1986)

$$\gamma_{mn}(\omega,d) = \frac{S_{mn}(\omega,d)}{\sqrt{S_{mm}(\omega,d)S_{nn}(\omega,d)}} = \left|\gamma_{mn}(\omega,d)\right|\exp\left[i\theta(\omega,d)\right] \tag{5}$$

where $S_{mn}(\omega,d)$ is the cross-power spectral density function of supports m and n; $S_{mm}(\omega,d)$ and $S_{nn}(\omega,d)$ are the power spectral density functions of supports m and n, respectively, which are functions of the angular frequency ω and station-to-station distance d; and $\exp[i\theta(\omega,d)]$ is used to describe

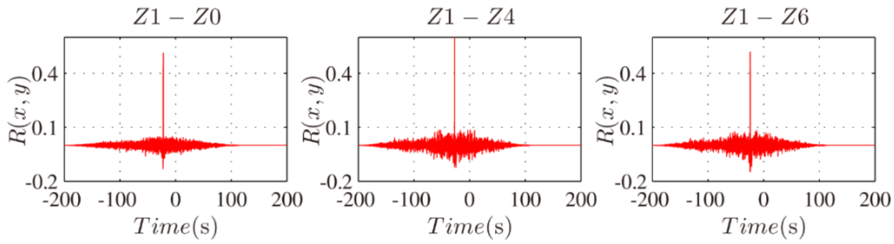

Fig. 9 Cross-correlation function before arrival time perturbations are modified

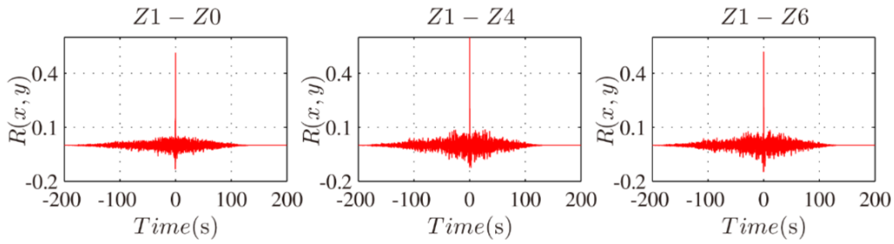

Fig. 10 Cross-correlation function after arrival time perturbations are modified

the wave passage effect, i.e., the delay in the arrival of the waveforms at the more distant station caused by the propagation of waveforms. The expression $|\gamma_{mn}(\omega,d)|$ is the lagged coherency, which is used to measure similarity in ground motion and varies from 0 to 1.

However, seismic ground motions across the dense array incorporate random time delay fluctuations associated with the wave passage delay, and these fluctuations vary for each recording station. These arrival time perturbations are caused by the upward travel of waves through horizontal variations in the geological structure below the array (Spudich 1994) and by deviations in the propagation patterns of the waves from that of plane wave propagation (Boissieres *et al*. 1995). The wave passage effects control the complex term in Eq. (5), and the arrival time perturbations affect its absolute value, namely, the lagged coherency. Therefore, the alignment of the data with respect to a reference station can be used to partially eliminate these effects in coherency estimates, that is, to remove wave passage effects (Zerva 2002).

In this process, a cross correlation of the motions relative to those at the reference station is performed. The time corresponding to the highest correlation provides a delay in the arrival of the waves at the various stations relative to their arrival at the reference station. Once the motions are aligned, they become invariant to the reference station selection, but the value of the time delay required for alignment is relative, that is, it is affected by the choice of the reference station. In this study, station Z1 is selected as the reference station. The reason for this choice is that the relative elevation of Z1 is zero in several stations and the site condition is bedrock, which may help to avoid the influence of site and topographic conditions. The arrival time perturbations related to reference station Z1 are eliminated using Eq. (3). First, calculate the cross-correlation functions of two accelerations from Z1 and other station, as shown in Fig. 9 (take results between station Z1 and other stations (Z0, Z4 and Z6) for example). Then, determine the time corresponding to the highest correlation value, which provides a delay in the arrival of the wave relative to the reference record. Finally, keep the reference record unchanged, the acceleration time series from other stations is moved forward or backward along the time axis so that the maximum value of the cross-correlation function between two accelerations occurs at the zero point in time, as shown in Fig. 10.

We should emphasize that coherency estimates strongly depend on the type of smoothing window w(τ) and the amount of smoothing performed on the raw data. Abrahamson *et al*. (1991) noted that the choice of smoothing window should be based on not only the statistical properties of coherency but also the purpose for which it is derived. In this study, an 11-point Hamming window is used to calculate the coherency function. Evidently, very good agreement can be generally obtained, except for frequencies near zero.

After coherency estimates are obtained from the recorded time histories, a functional form (model) can be fitted based on the coherency data by means of regression analysis. In the following section, we discuss the variation of lagged coherency $|\gamma_{mn}(\omega,d)|$ with the frequency and separation distance d.

3.1 Variation of lagged coherency with frequency

Station Z0 of ZGSA is located at a soil site, and the others are located on rock sites. In addition, station Z1 is located at the foot of a hill. Because local site conditions and rapidly varying topography may affect the variations of the lagged coherency in ground motion, we compare the coherency variations of different station combinations in the following sections.

3.1.1 Stations Z0-Z1

The separation distance between stations Z0 and Z1 is only 51.57 m, and their elevation is the same. The lagged coherency between these stations as a function of frequency is illustrated in Fig. 11(a). The degressive trend of the lagged coherency with increasing frequency is clear when $f \leq 8.0$ Hz. At frequencies greater than 8.0 Hz, the curve

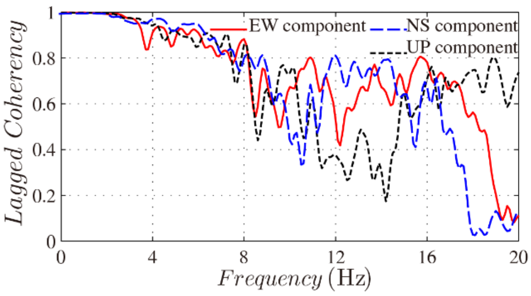

(a) Lagged coherency

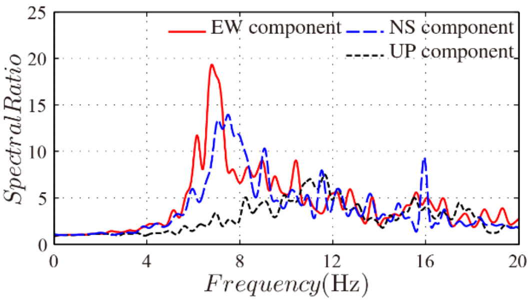

(b) Spectral ratios

Fig. 11 Plots showing the variation in lagged coherency and spectral ratios between stations Z0 and Z1 as functions of frequency

changes rapidly between peaks and valleys. These changes are related to the modulus of the spectral ratios of the two different sites, namely, $|F_m(i\omega)|/|F_n(i\omega)|$, as shown in Fig. 11(b). $|F_m(i\omega)|$ and $|F_n(i\omega)|$ are the Fourier amplitude spectra of sites *m* and *n*, respectively. Comparing Fig. 11(a) and Fig. 11(b), when the spectral ratios differ, the spatial ground motions at a local site are least correlated with a small value of lagged coherency near these frequencies. This result indicates that the lagged coherency is more difficult to model accurately at high frequencies than at low frequencies. Moreover, the variations in lagged coherency depend on the direction of ground motion. Specifically, the variation in the vertical component is different from those in the two horizontal components, but the variations in the two horizontal components are only slightly different.

Lagged coherency gradually decreases with increasing frequency (Spudich 1994, Zerva *et al*. 1997), but that determined from the Wenchuan event data exhibits a different trend. As shown in Fig. 11 (a), for the horizontal components, a brief increase occurs at approximately 10 Hz after obvious valleys in the curves. Then, the curves decline at frequencies greater than 17.5 Hz. For the vertical component, an obvious valley is observed at approximately 14 Hz, and the curve then continuously increases with increasing frequency. We suspect that this trend might be related to the local site conditions or topography because the site conditions of stations Z0 and Z1 are different and the local topography at station Z1 varies rapidly. Therefore, the variations in the lagged coherency related to station Z0 or station Z1 must be discussed separately.

3.1.2 Stations Z0-Z2, Z0-Z3 and Z0-Z6

The values of lagged coherency related to station Z0, the lone soil site, are computed to analyze the effects of different site conditions. Fig. 12 illustrates the lagged coherency variations of stations Z0-Z2 (d_{02}=70.98 m), stations Z0-Z3 (d_{03}=168.31 m) and stations Z0-Z6 (d_{06}=351.31 m) for EW, NS, and UP components, which are functions of frequency. A degressive trend in the lagged coherency can be observed with increasing frequency. However, the rate of coherency change differs in different directions and for various separation distances. In the same direction, the shorter the station-to-station distance is, the larger the frequency that creates obvious valleys (negative deflections) in the curves of the coherency functions, and the slower the rate of lagged coherency change.

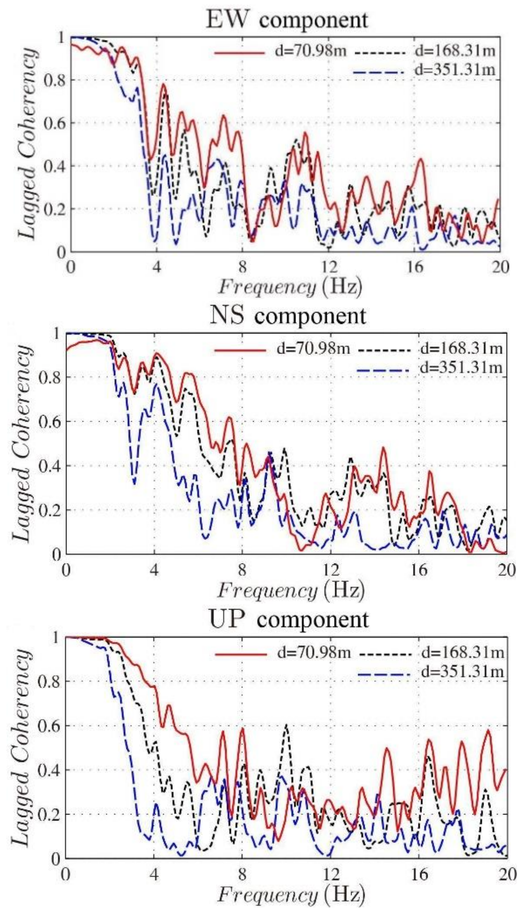

Fig. 12 Plots showing the variations in lagged coherency for stations Z0-Z2, Z0-Z3 and Z0-Z6 as functions of frequency

Moreover, rapidly changing peaks and valleys in the curves occur at high-frequency ranges, and these variations are related to the local site conditions. Fig. 13 plots the Fourier amplitude spectral ratios of stations Z0-Z2, stations Z0-Z3 and stations Z0-Z6 for EW, NS and UP components, respectively. Notably, when the values of the spectral ratios are relatively large, the values of lagged coherency are smaller near these frequencies. This result is expected because the lagged coherency measures the similarity between motions at two different locations. If two sites amplify the ground motions to the same extent at certain frequencies, the coherency loss is mainly caused by the incoherence effect and wave passage effect (Bi and Hao 2011). Changes in lagged coherency in high-frequency

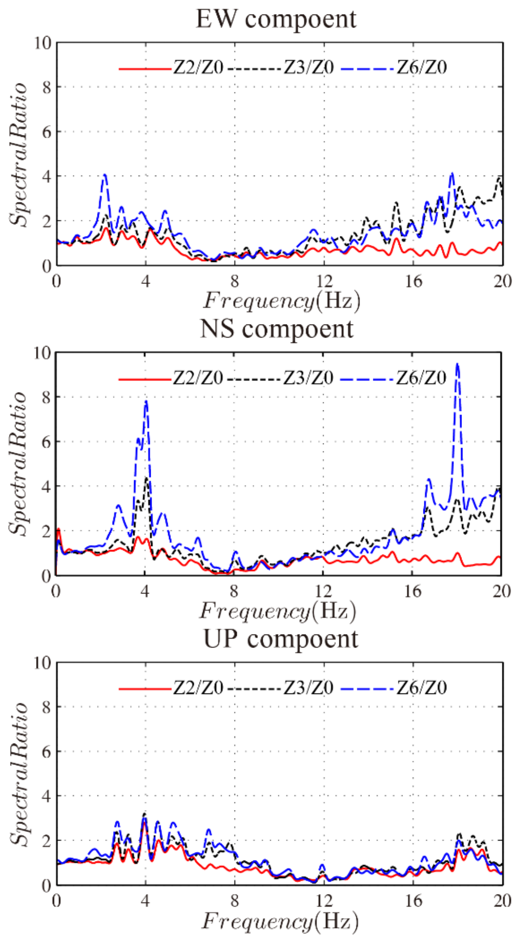

Fig. 13 Plots showing the variations in spectral ratios for stations Z0-Z2, Z0-Z3 and Z0-Z6 as functions of frequency

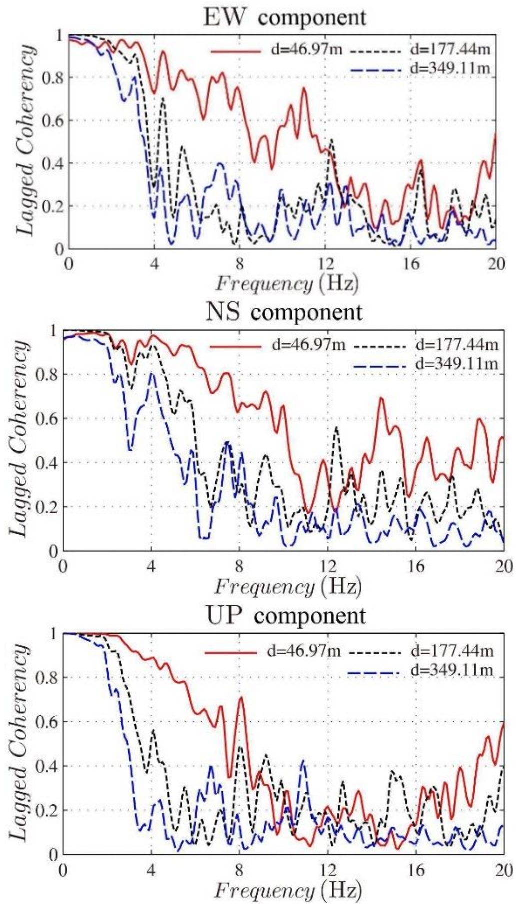

Fig. 14 Plots showing the variations in lagged coherency for stations Z1-Z2, Z1-Z4 and Z1-Z7 as functions of frequency

ranges are likely influenced by the different site conditions, but different site conditions have little influence on the lagged coherency trend with increasing frequency.

3.1.3 Stations Z1-Z2, Z1-Z4 and Z1-Z7

The values of lagged coherency related to station Z1 are calculated to observe the effect of neighboring topography because station Z1 is located at the foot of a hill with local topography that varies rapidly. The predominant frequencies of accelerations at station Z1 range from 0.6 -1.2 Hz for the NS component and from 0.4-1.8 Hz for the EW and UP components. Fig. 14 illustrates the variations in lagged coherency for stations Z1-Z2 (d_{12}=46.97 m), stations Z1-Z4 (d_{14}=177.44 m) and stations Z1-Z7 (d_{17}=349.11 m) with frequency changes for the three components. Note that the values of lagged coherency between stations Z1 and Z2 gradually increase with increasing frequency after an obvious valley. As the station-to-station separation distance increases, the variations gradually disappear. Therefore, we suspect that neighboring topography affects the coherency trend when the station-to-station distance is relatively small; however, as the interstation distance increases, this influence is gradually reduced.

3.2 Variation in lagged coherency with station-to-station distance

Assuming the frequency interval is Δf=0.05 Hzand the considered frequency ranges from 0.05 Hz to 20 Hz, the variation in the lagged coherence at each given frequency can be obtained. Fig. 15 shows the variations in lagged coherency along with the separation distance d at four given frequencies (f=0.5, 1.5, 5.0, and 10 Hz). The values related to station Z0 are denoted with asterisks (*), the values related to station Z1 are denoted with plus symbols (+), and those of other stations are denoted with circles (○). The following results can be seen from the figure:

(1) When f≤1.5 Hz, the values are generally greater than 0.8, especially in the vertical direction. When f>1.5 Hz, the degressive trend of the lagged coherency with increasing separation distance becomes significant, and the degressive rate of the vertical component is faster than those of the horizontal components.

(2) The variation in lagged coherency is affected by the different site conditions and neighboring topography in the frequency range of 2.5 Hz≤f≤5.0 Hz. Specifically, when f>25 Hz, the values related to stations Z0 and Z1 are less than those of the other stations, but the effect is not regular in the higher frequency range. This result indicates that wave propagation at a local site, even one with deterministic site properties, further reduces the cross correlation between spatial ground motions at rock sites.

(3) The variations in lagged coherency depend on the

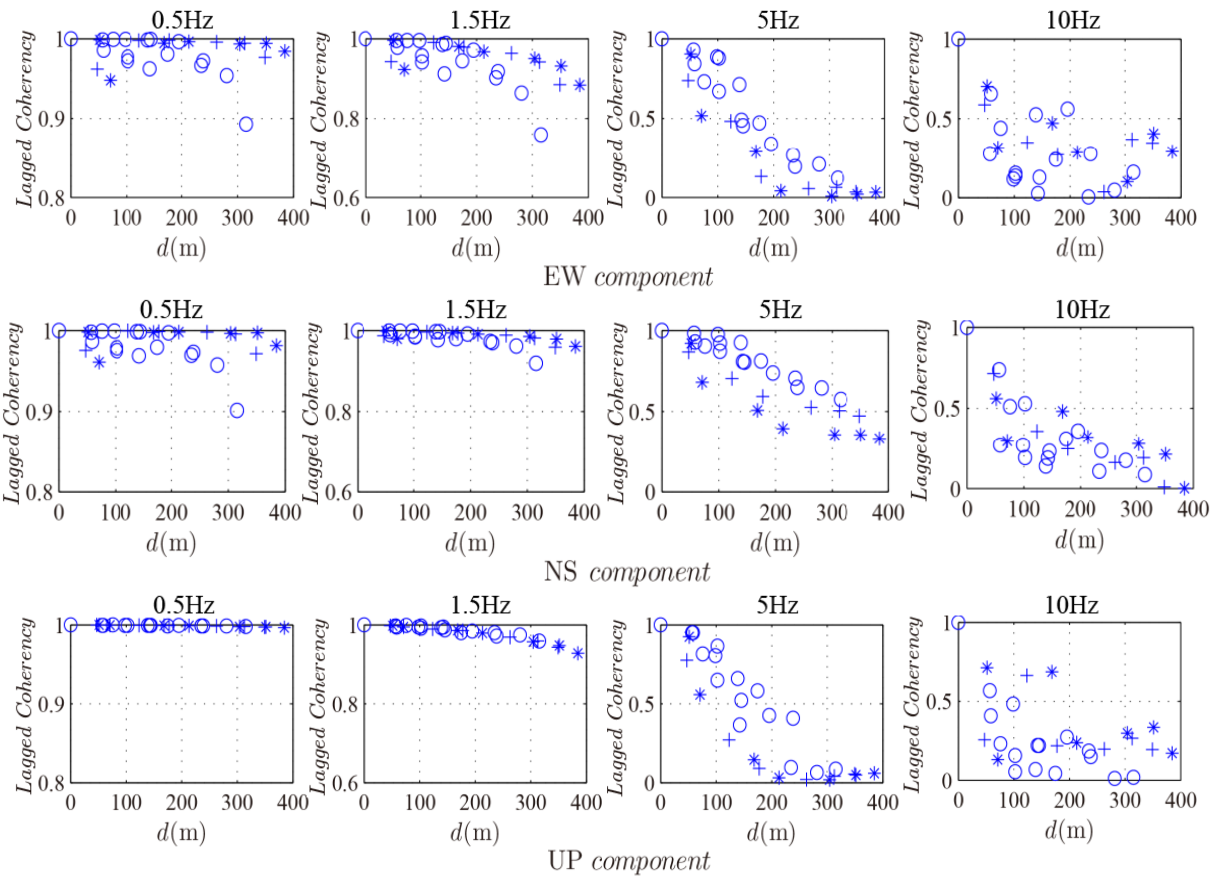

Fig. 15 Plots showing the variations in lagged coherency functions among stations as a function of separation distances when f=(0.5,1.5,5,10)Hz.The values related to station Z0 are denoted with asterisks (*), the values related to station Z1 are denoted with plus symbols (+), and the data from other stations are denoted with circles (○)

directions of the recordings because the degressive rate of the vertical component is faster than those of the two horizontal components. Nevertheless, the trends of the two horizontal components are only slightly different. Therefore, different models must be developed to simulate the variations in the lagged coherency of ground motion in the horizontal and vertical directions.

4. Data fitting and analysis based on exiting coherency models

4.1 Coherency simulation for the Wenchuan Earthquake

We first try to use the existing lagged coherency model to simulate the data from the Wenchuan event. Currently, two main types of lagged coherency models are used. One type includes empirical models obtained by analyzing strong-motion data recorded by dense seismography arrays. In this approach, model parameters are related to the site conditions of the array and can be used in similar cases. The second type includes semiempirical and semi-theoretical models, in which some functional forms are proposed based on theoretical analysis; however, the model parameters must be determined by analyzing actual seismic records. Therefore, accurately determining the best lagged coherency model is difficult. In this study, four models established by different methods are selected to simulate the variations in lagged coherency for the Wenchuan event. These models have been widely used to simulate the spatial correlation of multipoint ground motions. ***Model A*** was suggested by Feng and Hu (1981), and the parameters were obtained by analyzing strong-motion data recorded during the 1975 Haicheng earthquake in China. ***Model B*** was proposed by Harichandran and Vanmarcke (1986) based on the data from Event 20 in SMART-1. ***Model C*** was obtained based on a seismological method (Ding *et al.* 2004) that considered fault rupture in an elastic half space. This method is suitable for rock sites. ***Model D*** was developed by analyzing data from a dense seismograph array in the Adirondack Mountains (Menke *et al.* 1990).

The fitting results of these four models for the NS component of the Wenchuan earthquake at four frequencies (f=0.5, 1.5, 5.0, and 10 Hz) are shown in Fig. 16, in which the gray band represents the results of *Model D* because of its parameter range ($(0.4-0.7)\times10^{-3}$ sec/m)). The fitting results of these models are clearly affected by the frequency. *Model A* and *Model B* can provide satisfactory results in the high-frequency range, and *Model C* can yield satisfactory results in the low-frequency range. However, *Model D* seems to be inappropriate for the simulation of lagged coherency variations for the Wenchuan earthquake. Unfortunately, for the Wenchuan event, finding an existing

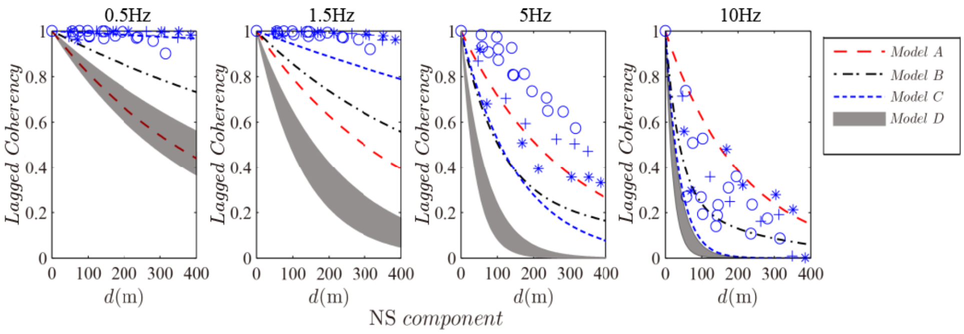

Fig. 16 Fitting results of models for NS components of the Wenchuan earthquake at f=(0.5,1.5,5,10)Hz. The gray band represents the results of *Model D* because of its parameter range (0.4−0.7)×10^{-3} sec/m). The values related to station Z0 are denoted with asterisks (*), the values related to station Z1 are denoted with plus symbols (+), and the data from other stations are denoted with circles (○)

Table 1 The details of the three additional earthquakes recorded by two seismographic arrays

Event	Mag.	Array	Station Num.	Year
27th	5.9	SMART-1	39	1984
San Simeon	6.5	UPSAR	14	2003
Parkfield	6.0	UPSAR	14	2004

Table 2 The coherency cut-off frequencies f_{cc} of the four earthquakes

Event	Wenchuan	27th	San Simeon	Parkfield
Epicentral distance (km)	226.6	135	55.6	11.6
f_{cc} (Hz)	1.5	1.0	0.75	0.50

model to simulate the coherency variations in the entire frequency range is difficult because the source-to-site distance of ZGSA is approximately 226.6 km. From the analysis presented in Section 3.2, the rate of lagged coherency degression with separation distance in the low-frequency range can be concluded to differ considerably from that in the high-frequency range. Therefore, a cut-off frequency exists, above and below which the rate of lagged coherency degression based on interstation distance differs. In this study, we name this cut-off frequency the 'coherency cut-off frequency' f_{cc}. Once the value of f_{cc} is determined, the coherency variations of ground motion can be fitted in different frequency ranges.

4.2 Coherency cut-off frequency

First, we discuss the factors that influence f_{cc} based on the lagged coherency data from the Wenchuan earthquake. Assuming that the frequency interval is Δf=0.05 Hz, the rate of lagged coherency degression based on the separation distance is calculated using simulation data corresponding to a series of given frequencies (f_i=f_{i-1}+Δf Hz). In this analysis, the data related to station Z0 are denoted with asterisks (*), the data related to station Z1 are denoted with plus symbols (+), and data from other stations are noted with circles (○). These data separately illustrate the effects of some factors on the variations in lagged coherency. The results show that above and below 1.5 Hz, the rates of lagged coherency degression based on the interstation distances are obviously different. In addition, f_{cc} is not affected by the site conditions and neighboring topography. Given the coherency analyses of other earthquakes (Yu *et al*. 2011), we suspect that the value of f_{cc} may be related to the source-to-site distance of ground motion. Therefore, we further select data from three additional earthquakes collected by two dense seismograph arrays to analyze the effect of source-to-site distance on the coherency cut-off frequency.

The details of the three earthquakes are listed in Table 1. The 2003 San Simeon and 2004 Parkfield earthquakes were recorded by the U.S. Geological Survey Parkfield Dense Seismograph Array (UPSAR), which includes 14 seismograph stations spaced irregularly over hilltops with an interstation spacing ranging from 25 m to approximately 960 m (Fletcher *et al*. 1992). The 27th event in Table 1 was recorded in 1984 by SMART-1, which contains 39 stations with spatial distances between stations ranging from 88.9 m to 4208.4 m. Similarly, the rates of lagged coherency degression based on separation distance for a series of given frequencies (f_i=f_{i-1}+0.05 Hz) were calculated. The results illustrate that the values calculated from near-field earthquakes decay faster than those from far-field earthquakes as the separation distance increases at low frequency. In the high-frequency range, the far-field values decay more rapidly than those in at low frequencies with increasing separation distance. Similar results were found by Somerville *et al.* (1988) and Abrahamson *et al.* (1991a). Notably, the above analysis shows that the coherency cut-off frequency is related to the source-to-site distance, which decreases as the epicentral distance decreases. For the Wenchuan earthquake, the value of f_{cc} can be set to 1.5 Hz, but for the Parkfield earthquake, with a source-to-site distance of 11.6 km, this value is approximately 0.5 Hz. By comparing and analyzing these data, the coherency cut-off frequencies related to the source-to-site distance are determined, as are listed in Table 2.

5. Parametric modeling of lagged coherency for ground motions

5.1 Piecewise model based on coherency cut-off frequency

According to the above analysis, we conclude that satisfactory fitting results can be obtained if different model parameters are used for different frequency ranges. Therefore, a piecewise model based on the coherency cut-off frequency is proposed to simulate the variations in the lagged coherency of ground motions, that is

$$|\gamma(\omega,d)| = \frac{1}{1+\alpha(f_{cc})d^{q(f_{cc})}\omega^4}\exp[-\beta(f_{cc})d] \tag{6}$$

This model is a rational expression that relates the angular frequency ω and station-to-station distance d. Parameters $\alpha(f_{cc})$, $q(f_{cc})$ and $\beta(f_{cc})$ are related to the coherency cut-off frequency f_{cc} defined in this study.

The choice of such a model form is based on a consideration that can obtain the analytical solutions of correlation coefficients among modes and supports in the response spectrum method when individual supports of extensive structures undergo different motions in dynamic response analysis. Using analytical solutions for correlation coefficients can improve the computational efficiency of the dynamic analysis of large structures. For a linear damping system, the analytical solutions of three cross-correlation coefficients can be calculated by the residue theorem

$$\rho_{umun} = \frac{\lambda_{umun}}{\sigma_{u_m}\sigma_{u_n}},\ \rho_{umjn} = \frac{\lambda_{umjn}}{\sigma_{u_m}\sigma_{q_{jn}}},\ \rho_{q_{im}q_{jn}} = \frac{\lambda_{imjn}}{\sigma_{q_{im}}\sigma_{q_{jn}}} \tag{7}$$

in which

$$\lambda_{umun} = \int_{-\infty}^{\infty}\frac{1}{\omega^4}S_{u_m u_n}(\omega,d)d\omega \tag{7a}$$

$$\lambda_{umjn} = -\int_{-\infty}^{\infty}\frac{1}{\omega^2}H_j(-i\omega)S_{u_m u_n}(\omega,d)d\omega \tag{7b}$$

$$\lambda_{imjn} = \int_{-\infty}^{\infty}H_i(i\omega)H_j(-i\omega)S_{u_m u_n}(\omega,d)d\omega \tag{7c}$$

where $\sigma_{u_m} = \sqrt{\lambda_{umum}}$ and $\sigma_{q_{im}} = \sqrt{\lambda_{imim}}$ represent the mean square roots of the support and modal displacement responses, respectively; $H_i(i\omega) = -\left(\omega_i^2 - \omega^2 + 2i\omega_i\zeta_i\omega\right)^{-1}$ is the frequency response function of mode i, in which ω_i and ζ_i are the free vibration frequency and critical damping ratio of the i th mode, respectively; and $S_{u_m u_n}(\omega,d)$ denotes the cross-power spectral density of processes u_m and u_n. Integrating over the frequency domain $-\infty<\omega<\infty$, the mean square response is obtained as $S_{u_m u_n}(\omega,d)$, which is the real-valued cross-power spectral density of acceleration processes and can be determined by Eq. (5).

In engineering-scale applications, the power spectral density functions of supports m and n can be assumed consistent

$$S(\omega) = \frac{\omega^4}{\omega^4+\omega_c^4}\frac{\omega_g^4+4\zeta_g^2\omega_g^2\omega^2}{\left(\omega^2-\omega_g^2\right)^2+4\zeta_g^2\omega_g^2\omega^2} \tag{8}$$

where ω_c, g_i and ζ_g are the frequency and damping ratios related to the site.

Based on the residue theorem, substituting Eq. (6) and Eq. (8) into Eq. (7) yields the following expression.

$$\lambda = -2\pi i\sum_{im(\omega_p)<0}\left[\frac{B(\omega_p)}{A(\omega_p)}\right] \tag{9}$$

Let $Q_1 = \alpha(f_{cc})d^{(f_{cc})}$, $Q_2 = \beta(f_{cc})d$, $\theta_c = \frac{\pi}{4}$, $\theta_g = \arcsin(\zeta_g)$ and $\theta_j = \arcsin(\zeta_j)$; then, λ_{umn} can be calculated by Eq. (10) using the 6 poles in the lower half plane, λ_{umjn} can be obtained by Eq. (11) using the 8 poles in the lower half plane, and λ_{imjn} can be determined by Eq. (12) with the 8 poles in the lower half plane (Yu *et al.* 2012), that is

$$\begin{aligned} A(\omega_p) &= Q_1\prod_{l=1,l\neq p}(\omega_p-\omega_l) \\ B(\omega_p) &= \left(\omega_g^4+4\zeta_g^2\omega_g^2\omega_p^2\right)e^{-[Q_2+i\omega_p T]} \end{aligned} \tag{10}$$

and the 6 poles are shown as $\omega_{p1} = \omega_c e^{i5\theta_c}$, $\omega_{p2} = \omega_c e^{i7\theta_c}$, $\omega_{p3} = \omega_g e^{-i\theta_g}$, $\omega_{p4} = -\omega_g e^{i\theta_g}$, $\omega_{p5} = Q_1^{1/4}e^{i5\theta_c}$ and $\omega_{p6} = Q_1^{1/4}e^{i7\theta_c}$.

$$\begin{aligned} A(\omega_p) &= Q_1\prod_{l=1,l\neq p}(\omega_p-\omega_l) \\ B(\omega_p) &= \omega_p^2\left(\omega_g^4+4\zeta_g^2\omega_g^2\omega_p^2\right)e^{-[Q_2+i\omega_p T]} \end{aligned} \tag{11}$$

and the 8 poles are listed as $\omega_{p1} = \omega_c e^{i5\theta_c}$, $\omega_{p2} = \omega_c e^{i7\theta_c}$, $\omega_{p3} = \omega_g e^{-i\theta_g}$, $\omega_{p4} = -\omega_g e^{i\theta_g}$, $\omega_{p5} = Q_1^{1/4}e^{i5\theta_c}$, $\omega_{p6} = Q_1^{1/4}e^{i7\theta_c}$, $\omega_{p7} = \omega_j e^{-i\theta_j}$ and $\omega_{p8} = -\omega_j e^{i\theta_j}$.

$$\begin{aligned} A(\omega_p) &= Q_1\prod_{l=1,l\neq p}(\omega_p-\omega_l) \\ B(\omega_p) &= \omega_p^4\left(\omega_g^4+4\zeta_g^2\omega_g^2\omega_p^2\right)e^{-[Q_2+i\omega_p T]} \end{aligned} \tag{12}$$

and the 8 poles are listed as $\omega_{p1} = \omega_c e^{i5\theta_c}$, $\omega_{p2} = \omega_c e^{i7\theta_c}$, $\omega_{p3} = \omega_g e^{-i\theta_g}$, $\omega_{p4} = -\omega_g e^{i\theta_g}$, $\omega_{p5} = Q_1^{1/4}e^{i5\theta_c}$, $\omega_{p6} = Q_1^{1/4}e^{i7\theta_c}$, $\omega_{p7} = \omega_j e^{-i\theta_j}$ and $\omega_{p8} = -\omega_j e^{i\theta_j}$.

5.2 Fitting of model parameters

The model parameters $\alpha(f_{cc})$, $q(f_{cc})$ and $\beta(f_{cc})$ of Eq. (6) can be obtained by regression analysis of data recorded by the dense seismography array. From the above coherency analysis of ground motion, we know that the rate of lagged coherency degression in the vertical direction is faster than those in the two horizontal directions. However, the degression rates of the two horizontal components are only slightly different. Therefore, the fitting of data recorded by the array considers two directions: the horizontal and vertical directions.

(a) Wenchuan earthquake recorded by ZGSA

The parameters $\alpha(f_{cc})$, $q(f_{cc})$, and $\beta(f_{cc})$ obtained by fitting data recorded by ZGSA during the Wenchuan earthquake for horizontal and vertical directions are listed in Table 3. This set of parameters is suitable for coherency simulations of the far-field earthquake because the source-to-site distance of ZGSA is approximately 226.6 km. Moreover, because variations in the lagged coherency are

Table 3 Model parameters of Wenchuan earthquake recorded by ZGSA

Comp.	Site	Freq. (Hz)	$\alpha(f_{cc})$	$\beta(f_{cc})$	$q(f_{cc})$
Hor.	Rock Mixed	$f \le 1.5$	1.15×10^{-8}	6.39×10^{-5}	0.80
Ver.	Rock Mixed	$f \le 1.5$	9.16×10^{-12}	1.45×10^{-5}	2.31
Hor.	Rock	$f > 1.5$	1.50×10^{-9}	1.70×10^{-4}	1.29
	Mixed		3.03×10^{-11}	1.94×10^{-4}	1.93
Ver.	Rock	$f > 1.5$	6.78×10^{-12}	3.59×10^{-5}	2.27
	Mixed		7.78×10^{-12}	7.59×10^{-5}	2.59

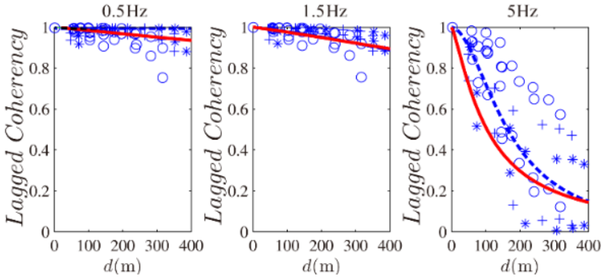

(a) Horizontal direction

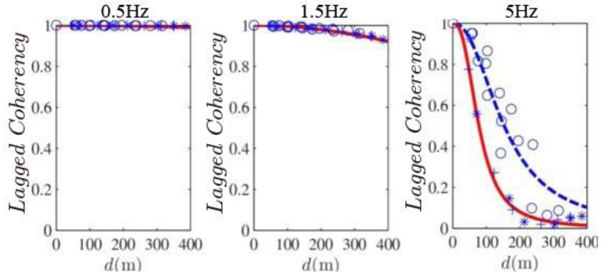

(b) Vertical direction

Fig. 17 Fitting results for the Wenchuan earthquake. The values related to station Z0 are denoted with asterisks (*), the values related to station Z1 are denoted with plus symbols (+), and the data from other stations are denoted with circles (○). The solid line represents the results for mixed site (soil over rock) and the dotted line represents the results for rock site

affected by the different site conditions and neighboring topography in the high-frequency range, the values related to stations Z0 and Z1 are less than those at other stations, as shown in Fig. 15. Therefore, two sets of parameters are given according to whether the stations are located on sites with rock or mixed soil over rock. The fitting curves of Eq. (6) for the Wenchuan event at three frequencies (f=0.5, 1.5 and 5.0 Hz) are shown in Fig. 17, in which the solid line represents the results for mixed site (soil over rock) conditions and the dotted line represents the results for rock sites. When using data from Wenchuan earthquake to fit model parameters, standard deviation is adopted to measure the fitting accuracy. The results show that the standard deviation in both the low-frequency and high-frequency ranges are all less than 0.3, that is, the fitting results of the piecewise model proposed in this study are satisfactory in the frequencies of engineering concern.

Table 4 Model parameters of the 27th earthquake recorded by SMART-1

Comp.	Freq. (Hz)	$\alpha(f_{cc})$	$\beta(f_{cc})$	$q(f_{cc})$
Hor.	$f \le 1.0$	-3.73×10^{-11}	2.01×10^{-4}	1.90
Ver.		2.38×10^{-4}	3.96×10^{-4}	2.31×10^{-2}
Hor.	$f > 1.0$	2.85×10^{-8}	1.82×10^{-4}	5.42×10^{-1}
Ver.		1.18×10^{-6}	3.81×10^{-4}	2.04×10^{-12}

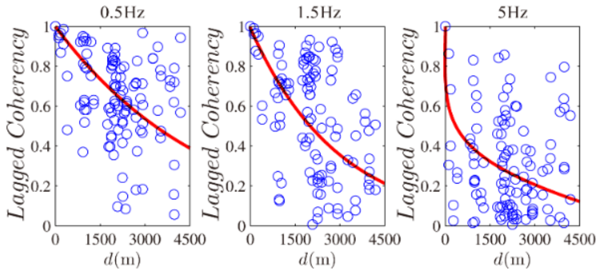

(a) Horizontal direction

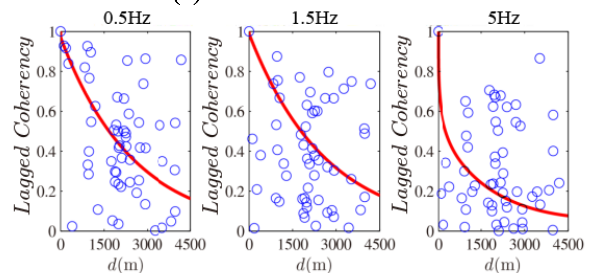

(b) Vertical direction

Fig. 18 Fitting results for the 27th event recorded by SMART-1. The results from recordings are denoted with circles (○). The solid line represents the fitting curves.

(b) The 27th earthquake recorded by SMART-1

The parameters in Eq. (6) obtained by fitting data from the 27th event recorded by SMART-1 are listed in Table 4, in which the coherency cut-off frequency is approximately 1.0 Hz. The fitting curves of Eq. (6) at three frequencies (f=0.5, 1.5, and 5.0 Hz) in the horizontal and vertical directions are plotted in Fig. 18, in which solid line represents the fitting results of model. We still use standard deviation to measure fitting results. Compared with the fitting results of Wenchuan earthquake, the standard deviation obtained by fitting data from SMART-1 array is relatively large, but the fitting results are basically the same in the high and low frequency ranges. That is, satisfactory results are obtained by the piecewise model in whole frequency ranges.

(c) San Simeon and Parkfield Earthquakes recorded by UPSAR

The source-to-site distances of the 2003 San Simeon earthquake and 2004 Parkfield earthquake are approximately 55.6 km and 11.6 km, respectively. In addition, UPSAR is characterized by generally rocky site conditions. Therefore, the parameters obtained from the two earthquakes are suitable for the estimation of coherency variations in ground motion at rocky sites for a near-field earthquake.

The values of parameters $\alpha(f_{cc})$, $q(f_{cc})$, and $\beta(f_{cc})$ for the

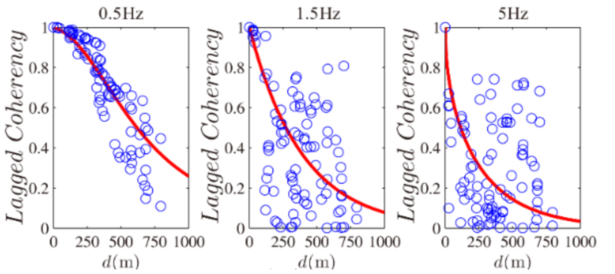

(a) Horizontal direction

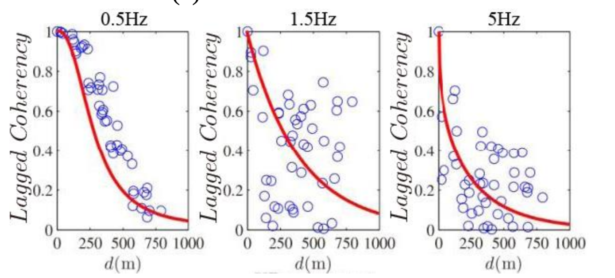

(b) Vertical direction

Fig. 19 Fitting results for the San Simeon earthquake recorded by UPSAR. The results from recordings are denoted with circles (○). The solid line represents the fitting curves

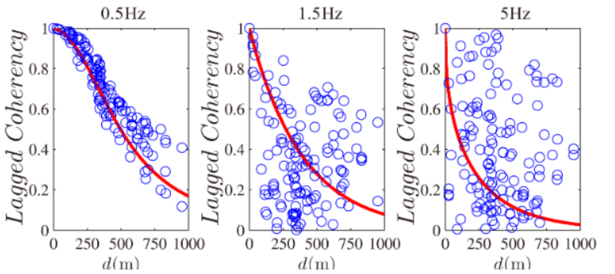

(a) Horizontal direction

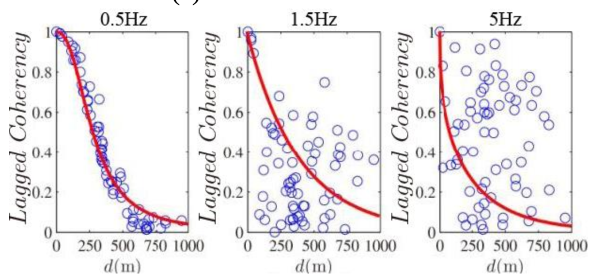

(b) Vertical direction

Fig. 20 Fitting results for the Parkfield earthquake recorded by UPSAR. The results from recordings are denoted with circles (○). The solid line represents the fitting curves

San Simeon and Parkfield earthquakes are listed in Table 5, in which the values of f_{cc} are 0.75 Hz and 0.5 Hz, respectively. The fitting curves of Eq. (6) for the San Simeon and Parkfield earthquakes at three frequencies (f=0.5, 1.5, and 5.0 Hz) in the horizontal and vertical directions are plotted in Fig. 19 and Fig. 20, respectively, in which solid lines represent the fitting results of model. The results show that the standard deviation obtained by fitting data from UPSAR is less than 0.2 in the low- frequency range, and in the high-frequency part, the fitting standard deviation is slightly larger, but not more than 0.3.

Table 5 Model parameters of the San Simeon and Parkfield earthquakes recorded by UPSAR

Event	Comp.	Freq. (Hz)	$\alpha(f_{cc})$	$\beta(f_{cc})$	$q(f_{cc})$
San Simeon	Hor.	$f \le 0.75$	6.42×10^{-9}	2.22×10^{-4}	2.15
	Ver.		6.42×10^{-9}	2.22×10^{-4}	2.31
	Hor.	$f > 0.75$	5.52×10^{-8}	2.53×10^{-3}	0.45
	Ver.		5.52×10^{-8}	2.53×10^{-3}	0.45
Parkfield	Hor.	$f \le 0.5$	5.06×10^{-9}	1.85×10^{-4}	2.23
	Ver.		6.42×10^{-9}	2.22×10^{-4}	2.45
	Hor.	$f > 0.5$	5.52×10^{-8}	2.53×10^{-3}	0.45
	Ver.		5.52×10^{-8}	2.53×10^{-3}	0.45

Therefore, good simulation results in the whole frequency ranges can still be obtained by using the model piecewise model developed in this study.

5.3 Discussion

The lagged coherency model has been used not only directly to provide input motions at the supports of lifelines in random vibration analyses, but also to simulate the spatial correlation of multipoint ground motions. Generally, researchers have chosen the appropriate model and parameters based on conditions similar to the dense seismography array to carry out the corresponding studies. Given the above analysis, we suspect that the model parameters can be selected based on the source-to-site distance. For this reason, we compare the models proposed in this paper with the existing models under similar conditions and certain source-to-site distances. However, considering that the source-to-site distances of the existing models are not more than 120 km, finding any existing model to compare to the results from ZGSA is difficult because the distance from ZGSA to the epicenter is approximately 226.6 km. Considering that many lagged coherency models have been established based on abundant recordings from SMART-1, we therefore select existing models to analyze the parameters obtained from the 27th earthquake recorded by SMART-1. Accordingly, two models are selected based on the similarity of earthquake records. One is the Hao and Oliveira model (1989) obtained based on the data from Event 20 in SMART-1 (the source-to-site distance is approximately 116km). The other is the Yang and Chen model (2000), which was obtained based on the data from Event 25 in SMART-1 (the source-to-site distance is approximately 100km). Fig. 21 compares the difference between the fitting results of the model suggested in this study and the two existing models at three frequencies (f=0.5, 4.0 and 6.0 Hz). The results obtained by the three models are relatively close. However, the curve of the piecewise model with the station-to-station distance decays faster than those from the other two models in the high-frequency range, but the low-frequency range shows the opposite behavior. From the analysis in Section 3.2, the local site conditions may clearly reduce the cross correlation in the high-frequency range, so the parameters listed in Table 4 are more appropriate to estimate the spatial variations of ground motion at local sites with conditions

Table 6 The details of existing lagged coherency models

Model name	Array	Event	Epicentral distance (km)
Hao and Oliveira (1989)	SMART-1	46th	79.0
Hao and Oliveira (1989)	SMART-1	47th	79.0
Yang and Chen (2000)	SMART-1	46th	79.0
Loh and Lin (1990)	SMART-1	40th	68.1
Loh and Lin (1990)	MART-1	45th	76.1

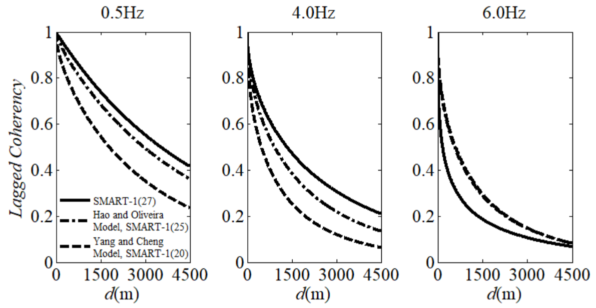

Fig. 21 Comparison between the fitting results for the 27th event recorded by SMART-1 and the existing model results

similar to those of SMART-1 and source-to-site distances of approximately 100 -140 km.

Moreover, we attempted to find a similar model to compare the results obtained from the San Simeon and Parkfield earthquakes, as listed in Table 5, but in the source-to-site distance ranges of 40-80 km and 0-30 km, existing models similar to the site conditions of UPSAR cannot be found. Therefore, we ignore the effect of the site conditions to choose suitable models based on the source-to-site distance ranges of 40 - 80 km to compare to the results obtained from the San Simeon earthquake. The details of the five selected models are listed in Table 6. A comparison of the results between these models is plotted in Fig. 22. This figure shows that the results of the piecewise model are close to those of the Hao and Oliveira model (1989) as well as those of the Yang and Chen model (2000) in the low-frequency range, however, as the frequency increases, the results of the piecewise model are close to those of the Loh and Lin model (1990) based on the 40th and 45th Events recorded by SMART-1. Because the rate of lagged coherency degression with the station-to-station distance in the high-frequency range is faster than that in the low-frequency range, the parameters presented in Table 5 seem more reasonable to approximately estimate the spatial variation in ground motion across the entire frequency range.

Through the above comparison and analysis, the model parameters can clearly be selected from the source-to-site distances for simulating the spatial variation of ground motion. Therefore, the parameters from the Wenchuan earthquake, as listed in Table 3, can be used to simulate the lagged coherency variation in ground motion at rock and mixed sites for a far-field earthquake. The parameters listed in Table 4 are suitable for estimating the spatial variations of ground motion at local sites with conditions similar to those of SMART-1 and source-to-site distances of approximately 100-140 km. The parameters listed in Table

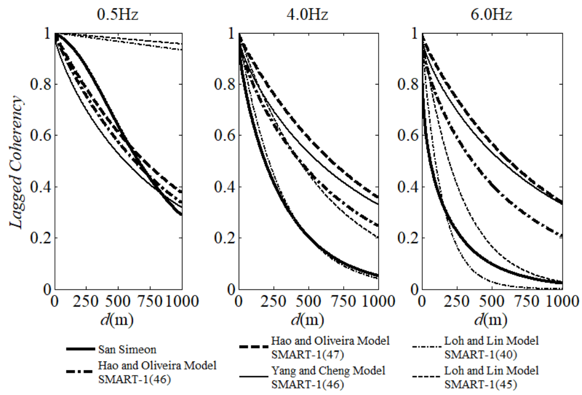

Fig. 22 Comparison between the fitting results for the San Simeon earthquake recorded by UPSAR and the existing model result

5 are suitable for the estimation of coherency variations in ground motion at rock sites for a near-field earthquake. Conclusively, the piecewise model developed in this study provides a good choice for approximately simulating the spatial variations in ground motions at local sites with known source-to-site distances. In addition, for structural seismic analysis and design, these models can be used to simulate multi-point ground motions that can characterize spatial correlation characteristics. Also, these models can be directly used in the response spectrum method when individual supports of extensive structures undergo different motions in dynamic response analysis, in which analytical solutions of correlation coefficients among modes and supports can be obtained to improve the computational efficiency of the dynamic analysis of large structures.

6. Conclusions

The analysis of the spatial variations in acceleration data recorded by ZGSA during the 2008 Ms 8.0 Wenchuan earthquake event leads to the following conclusions, definitions and model:

(1) The analysis of the amplitude spectra variations in accelerations recorded by ZGSA during the Wenchuan event indicates that the variations in ground motions in the high-frequency range are mainly controlled by the neighboring topographic effects and the local site conditions, which have a larger effect in the horizontal direction than in the vertical direction.

(2) The variations in the lagged coherency of ground motion at high frequencies are influenced by different site conditions, which result in rapidly changing curve peaks and valleys. Nevertheless, local differences in site conditions have little influence on the lagged coherency trend with increasing frequency.

(3) Furthermore, neighboring topographic conditions affect the trend of the lagged coherency with increasing frequency when the station-to-station distance is relatively small. However, as the interstation distance increases, the influence gradually decreases.

(4) We define the 'coherency cut-off frequency', which is related to the source-to-site distance, to distinguish the

rate of lagged coherency variation based on the separation distance in the low-frequency and high-frequency ranges. We analyze four earthquakes with different source-to-site distances and determine the values of the coherency cut-off frequency.

(5) A new piecewise model is presented to simulate the variations in the lagged coherency of ground motion with parameters suitable for earthquakes in the near and far fields. This model is related to the coherency cut-off frequency and can effectively reflect the changes in lagged coherency of ground motions based on frequency and separation distance changes. This model provides a good choice for simulating the spatial variations in ground motions at local sites with known source-to-site distances.

Acknowledgements

The financial supports from Natural Science Foundation of China (No. 51878627 and No. 51478440) are much appreciated.

References

Abrahamson, N.A., Schneider, J.F. and Step, J.C. (1991), "Spatial coherency of shear waves from the Lotung, Taiwan large-scale seimic test", *Struct. Saf.*, **10**, 145-162. https://doi.org/10.1016/0167-4730(91)90011-W.

Abrahamson, N.A., Schneider, J.F. and Step, J.C. (1991a), "Empirical spatial coherency functions for applications to soil-structure interaction analyses", *Earthq. Spectra*, **7**, 1-28. https://doi.org/10.1193/1.1585610.

Amiri, G.G. and Bagheri, A. (2009), "Simulation of earthquake records using combination of wavelet analysis and non-stationary Kanai-Tajimi model", *Struct. Eng. Mech.*, **33**(2), 179-1961. https://doi.org/10.12989/sem.2009.33.2.179.

Bi, K.M. and Hao, H. (2011), "Influence of irregular topography and random soil properties on coherency loss of spatial seismic ground motions", *Earthq. Eng. Struct. Dyn.*, **40**, 1045-1061. https://doi.org/10.1002/eqe.1077.

Bi, K.M. and Hao, H. (2012), "Influence of ground motion spatial variations and local soil conditions on the seismic responses of buried segmented pipelines", *Struct. Eng. Mech.*, **44**(5), 663-680. I: http://dx.doi.org/10.12989/sem.2012.44.5.663.

Bilici, Y., Bayraktar, A. and Adanur, S. (2009), "Comparison of uniform and spatially varying ground motion effects on the stochastic response of fluid-structure interaction systems", *Struct. Eng. Mech.*, **33**(4), 407-428. https://doi.org/10.12989/sem.2009.33.4.407.

Boissieres, H.P. and Vanmarcke, E.H. (1995), "Estimation of lags for a seismograph array: wave propagation and composite correlation", *Soil Dyn. Earthq. Eng.*, **14**, 5-22. https://doi.org/10.1016/0267-7261(94)00026-D.

Bolt, B.A., Loh, C.H., Penzien, J., Tsai, Y.B. and Yeh, Y.T. (1982), "Preliminary report on Smart 1. Strong motion array in Taiwan", Earthquake Engineering Research Center, Report No. UCB/EERC87/13, University of California, Berkeley, CA.

Boore, D.M. (2001), "Effect of baseline correlation on displacement and response spectra for several recordings of the 1999 Chi-Chi, Taiwan, earthquake", *Bull. Seismol. Soc. Am.*, **91**, 1199-1211. https://doi.org/10.1785/0120000703.

Bozorgnia, Y. and Campbell, K.W. (2004), "The vertical to horizontal response spectral ratio and tentative procedures for developing simplified V/H vertical design spectra", *J. Earthq. Eng.*, **8**(2), 175-207.

Bradley, B.A. and Cubrinovski, M. (2011), "Near-source strong ground motions observed in the 22 February 2011 Christchurch earthquake", *Bull. NZ. Soc. Earthq. Eng.*, **44**(4), 181-194. https://doi.org/10.1785/gssrl.82.6.853.

Chaouch, K.A., Tiliouine, B., Hammoutence, M., Sigbjoronsson, R. and Rupakhety, R. (2016), "Estimateing ground motion incoherence thought finite source simulation: a case study of 1980 EI-Aanam Earthquake", *Bull. Earthq. Eng.*, **14**, 1195-1217. https://doi.org/10.1007/s10518-016-9867-x.

Der Kiureghian, A. (1996), "A coherency model for spatially varying ground motions", *Earthq. Eng. Struct. Dyn.*, **25**, 99-111. https://doi.org/10.1002/(SICI)1096-9845(199601)25:1<99::AID-EQE540>3.0.CO;2-C.

Ding, H.P., Liu, Q.F., Jin, X. and Yuan, Y.F. (2004), "A coherency function model of ground motion at base rock corresponding to strike-slip fault", *Earthq. Sci.*, **17**(1), 64-69. https://doi.org/10.1007/BF03191396.

Feng, Q.M. and Hu, Y.X. (1981), "Spatial correlation model of ground motion", *Earthq. Eng. Eng. Vib.*, **1**, 1-8.

Fletcher, J.B., Baker, M., Spudich, P., Goldstein, P., Sims, J.D. and Hellweg, M. (1992), "The USGS Parkfield, California, dense seismograph array, UPSAR", *Bull. Seismol. Soc. Am.*, **82**(2), 1041-1070.

Gade, M. and Raghukanth, S.T.G. (2018), "Spatial variation of ground rotational motions in elastic half-space", *Soil Dyn. Earthq. Eng.*, **107**, 66-76. https://doi.org/10.1016/j.soildyn.2018.01.007.

Hao, H., Oliveira, C.S. and Penzien, J. (1989), "Multiple-station ground motion processing and simulation based on SMART-1 array data", *Nucl. Eng. Des.*, **111**(3), 293-310. https://doi.org/10.1016/0029-5493(89)90241-0.

Harichandran, R.S. and Vanmarcke, E.H. (1986), "Stochastic variation of earthquake ground motion in space and time", *J. Eng. Mech.*, **112**, 154-174. https://doi.org/10.1061/(ASCE)0733-9399(1986)112:2(154).

Hindy, A. and Novak, M. (1980), "Response of pipelines to random ground motion", *J. Eng. Mech.*, **106**, 339-360.

Hu, L., Xu, Y.L. and Zheng, Y. (2012), "Condition simulation of spatially variable seismic ground motions based on evolutionary spectra", *Earthq. Eng. Struct. Dyn.*, **41**, 2125-2139. https://doi.org/10.1002/eqe.2178.

Jankowski, R. and Wilde, K. (2000), "A simple method of conditional random field simulation of ground motions for long structures", *Eng. Struct.*, **22**(5), 552-561. https://doi.org/10.1016/S0141-0296(98)00125-4.

Jenkins, G.M. and Watts, D.G. (1969), "Spectral analysis and its applications", *J. Am. Statist. Associat.*, **64**(328), 174-175.

Konakli, K. and Der Kiureghian, A. (2012), "Simulation of spatially varying ground motions including incoherence, wave-passage and differential site-response effects", *Earthq. Eng. Struct. Dyn.*, **41**, 495-513. https://doi.org/10.1002/eqe.1141.

Liao, S. and Li, J. (2002), "A stochastic approach to site-response component in seismic ground motion coherency mode", *Soil Dyn. Earthq. Eng.*, **22**, 813-820. https://doi.org/10.1016/S0267-7261(02)00103-3.

Liao, S., Zerva, A. and Stephenson, W.R. (2007), "Seismic spatial coherency at site with irregular subsurface topography", *Prob. Appl. Geotech. Eng.*, ASCE, 1-10. https://doi.org/10.1061/40914(233)11.

Liu, G.H., Lian, J.J., Liang, C. and Zhao, M. (2017), "An effective approach for simulating multi-support earthquake underground motions", *Bull. Earthq. Eng.*, **15**, 4635-4659. https://doi.org/10.1007/s10518-017-0153-3.

Loh, C.H. and Lin, S.G. (1990), "Directionality and simulation in spatial variation of seismic waves", *Eng. Struct.*, **12**(2), 134-143.

https://doi.org/10.1016/0141-0296(90)90019-O.

Lou, C.H. (1985), "Analysis of the spatial variation of seismic waves and ground movements from SMART-1 data", *Earthq. Eng. Struct. Dyn.*, **13**, 561-581. https://doi.org/10.1002/eqe.4290130502.

Luco, J.E. and Wong, H.L. (1986), "Response of a rigid foundation to a spatially random ground motion", *Earthq. Eng. Struct. Dyn.*, **14**, 891-908. https://doi.org/10.1002/eqe.4290140606.

Menke, M., Lerner-Lam, A.L., Dubendorff, B. and Pacheco, J. (1990), "Polarization and coherence of 5 to 30Hz seismic wave fields at a hard-rock site and their relevance to velocity heterogeneities in the crust", *Bull. Seismol. Soc. Am.*, **80**, 430-449.

Mohamed, A.S., Sunghyuk, G., Sung, G.C. and Dookie, K. (2015), "Seismic responses of base-isolated nuclear power plant structures considering spatially varying ground motions", *Struct. Eng. Mech.*, **54**(1), 169-188. http://dx.doi.org/10.12989/sem.2015.54.1.169.

Novak, M. and Hindy, A. (1980), "Seismic response of buried pipelines", *3rd Canadian Conf. on Earthquake Engineering*, Montreal, Canada.

O1iveira, C.S., Hao, H. and Penzien, J. (1991), "Ground motion modeling for multiple-input structural analysis", *Struct. Saf.*, **10**, 79-93. https://doi.org/10.1016/0167-4730(91)90007-V.

Qu, T.J., Wang, J.J. and Wang, Q.X. (1996), "The utility model of spatial variation of ground motion power spectrum", *Acta Seismol. Sinica*, **18**, 55-62.

Saxena, V., Deodatis, G. and Shinozuka, M. (2000), "Effect of spatial variation of earthquake ground motion on the nonlinear dynamic responses of highway bridges", *Proc. of 12th World Conf. on Earthquake Engineering*, Auckland, New Zealand.

Sayed, M.A., Go, S., Cho, S.G. and Kim, D. (2015), "Seismic responses of base-isolated nuclear power plant structures considering spatially varying ground motions", *Struct. Eng. Mech.*, **54**(1), 169-188. https://doi.org/10.12989/sem.2015.54.1.169.

Somerville, P.G., Irikura, K., Graves, R., Sawada, S., Kagawa, T. and Smith, N. (1999), "Characterizing crustal earthquake slip models for the prediction of strong ground motion", *Seismol. Res. Lett.*, **70**(1), 59-80. https://doi.org/10.1785/gssrl.70.1.59.

Somerville, P.G., Mclaren, J.P. and Saikai C.K. (1988), "Site-specific estimation of spatial incoherence of strong ground motion", *Proceedings Earthquake Engineering and Soil Dynamics II, Recent Advances in Ground-motion Evaluation*, ASCE, Park City, Utab.

Somerville, P.G., Mclaren, J.P., Sen, M.K. and Helmberger, D.V. (1991), "The influence of site conditions on the spatial incoherence of ground motions", *Struct. Saf.*, **10**(1), 1-13. https://doi.org/10.1016/0167-4730(91)90003-R.

Spudich, P. (1994), Recent Seismological Insights into the Spatial Variation of Earthquake Ground Motions, New Developments in Earthquake Ground Motion Estimation and Implications for Engineering Design Practice, ATC 35-1.

Tian, L., Gai, X., Qu, B., Li, H.N. and Zhang, P. (2018), "Influence of spatial variation of ground motions on dynamic responses of supporting towers of overhead electricity transmission systems: An experimental study", *Eng. Struct.*, **128**, 67-83. https://doi.org/10.1016/j.engstruct.2016.09.010.

Tonyali, Z., Ates, S. and Adanur, S. (2019), "Spatially variable effects on seismic response of the cable-stayed bridges considering local soil site conditions", *Struct. Eng. Mech.*, **70**(2), 143-152. https://doi.org/10.12989/sem.2019.70.2.143.

Wang, G.Q., Boore, D.M., Igel, H. and Zhou, X.Y. (2003), "Some observation on collocated and closely spaced strong ground motion records of the 1999 Chi-Chi, Taiwan, earthquake", *Bull. Seismol. Soc. Am.*, **93**, 674-693. https://doi.org/10.1785/0120020045.

Wang, G.Q., Tang, G.Q., Jackson, C.R., Zhou, X.Y. and Lin, Q.L. (2006), "Strong ground motions observed at the UPSAR during the 2003 M6.5 San Simeon and 2004 M6.0 Parkfield Earthquakes", *Bull. Seismol. Soc. Am.*, **96**(4B), 159-182. https://doi.org/10.1785/0120050802.

Wu, Y.X., Gao, Y.F., Zhang, N. and Li, A.Y. (2016), "Simulation of spatially varying ground motions in V-shaped symmetric canyons", *J. Earthq. Eng.*, **20**(6), 992-1010. https://doi.org/10.1080/13632469.2015.1010049.

Yang, Q.S. and Chen, Y.J. (2000), "Practical coherency model for spatially varying ground motions", *Struct. Eng. Mech.*, **9**(2), 141-152. https://doi.org/10.12989/sem.2000.9.2.141.

Yu, R.F., Yuan, M.Q. and Yu, Y.X. (2011), "Spatial coherency function of seismic ground motion based on UPSAR records", *Appl. Mech. Mater.*, **90-93**, 1586-1592. https://doi.org/10.4028/www.scientific.net/AMM.90-93.1586.

Yu, R.F., Zhou, X.Y. and Yuan, M.Q. (2012), "Dynamic response analysis of generally damped linear system with repeated eigenvalues", *Struct. Eng. Mech.*, **42**(4), 449-469. https://doi.org/10.12989/sem.2012.42.4.449.

Yurdakul, M. and Ates, S. (2018), "Stochastic responses of isolated bridge with triple concave friction pendulum bearing under spatially varying ground motion", *Struct. Eng. Mech.*, **65**(6), 771-784. https://doi.org/10.12989/sem.2018.65.6.771.

Zerva, A. (2009), *Spatial Variation of Seismic Ground Motions-Modeling and Engineering Applications*, CRC Press, New York.

Zerva, A. and Harada, T. (1997), "Effect of surface layer stochasticity on seismic ground motion coherency and strain estimations", *Soil Dyn. Earthq. Eng.*, **16**, 445-457. https://doi.org/10.1016/S0267-7261(97)00019-5.

Zerva, A. and Zervas, V. (2002), "Spatial variation of seismic ground motions: An overview", *Appl. Mech. Rev.*, **55**(3), 271-297. https://doi.org/10.1115/1.1458013.

CC